NUCLEAR INSTRUMENTS AND METHODS 151 (1978) 519-523 ; © NORTH-HOLLAND PUBLISHING CO.

DETERMINATION OF RESOLUTION FUNCTION FOR SCINTILLATOR IN (n, d) SCATTERING EXPERIMENT

PIERRE CHATELAIN, YASAR ONEL and JACQUES WEBER

Institut de Physique de l'Université, Rue A.-L. Breguet 1, CH-2000 Neuchâtel, Switzerland

Received 15 September 1977 and in revised form 10 November 1977

Associated particle time-of-flight system for the D(d, n)^{3}He reaction has been developed for studying the scattering of neutrons of 2.45 and 3.27 MeV on deuterium. The distribution of neutrons elastically scattered by deuterium is obtained from the recoil deuteron spectrum. We present the method used to obtain differential cross-section from recoil energy spectrum. Preliminary results are given.

1. Introduction

In our measurements and analysis of spin observables of the n–d system at low energies[1,2]) it appeared that the previous determination of the n–d differential cross-sections at low energies[3–8]) were not adequate for fitting the data with the available model, even the simplest fit with orthogonal polynomials was not significant. Therefore it was necessary to obtain more and accurate data in the range of $\cos\theta_{CM} = -0.7$ to -1.0 to decide on the validity of the assumption of the highest partial wave $l_{max} = 2$.

We have used the recoil energy spectrum method and after some corrections this spectrum could be directly related to the differential cross-section in the center of mass.

D(d, n)^{3}He reaction was used as a source of neutrons with energies of 2.45 and 3.27 MeV. Many of the background problems have been overcome by using the associated particle time-of-flight technique (T.O.F.). The basis of this technique is that detection of a ^{3}He particle from the D(d, n)^{3}He reaction in a given direction is associated with the emission of a neutron with known energy at known angle with respect to the deuteron beam. The pulses from the ^{3}He particle detector identify the instants of emission of the neutrons in a defined cone and so can be used as starts signals for the T.O.F. system, the stop signals being derived from the detection of the recoil deuterons.

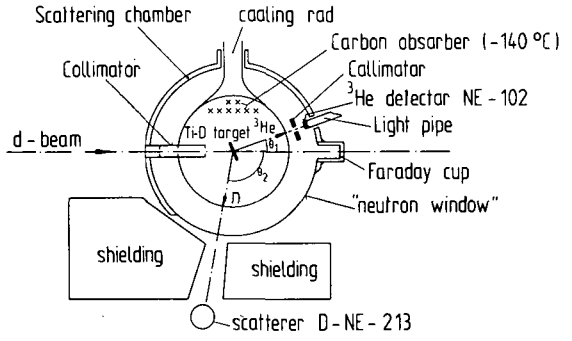

Fig. 1. Experimental set up. Typical values of angles and distances are: $\theta_1 = 30°$, $\theta_2 = 110°$, distance between target–^{3}He detector and target–scatterer: 30 and 66 cm, respectively.

In the two next sections we describe the experimental set-up, electronics and method used to obtain the differential cross-section following which we present the preliminary findings and results.

2. Experimental set-up

Fig. 1 shows the experimental arrangement devised so as to allow for neutron T.O.F. measurement and n–gamma discrimination, two essential features for getting clean data. The important pieces of equipment were: neutron source target, ^{3}He detector and deuterium scatterer.

The neutron source was the D(d, n)^{3}He reaction. The deuteron beam from our 3 MeV van de Graaff accelerator was impinging on a thin Ni-foil Ti–D target (Nukem, Hanau, Germany). (Ni-foil thickness: 0.5 μm; Ti thickness: 0.2 mg/cm^2; deuterium concentration equivalent: 1 Ci/in^2 tritium).

This target without cooling was able to stand up to 0.5 μA on a spot of 2 mm in diameter without any observable deterioration with time (simple calculation showed that the limit of 200 °C would have been reached with a beam intensity of about 1 μA). The ^{3}He detector was a NE-102 plastic scintillator, 2 mm in diameter, 0.5 mm thick, cemented to a plexiglass light-pipe, itself connected to a photomultiplier tube 56 AVP through a silicone oil joint. To prevent the target from carbon deposit, the scattering chamber was fitted with a dish filled

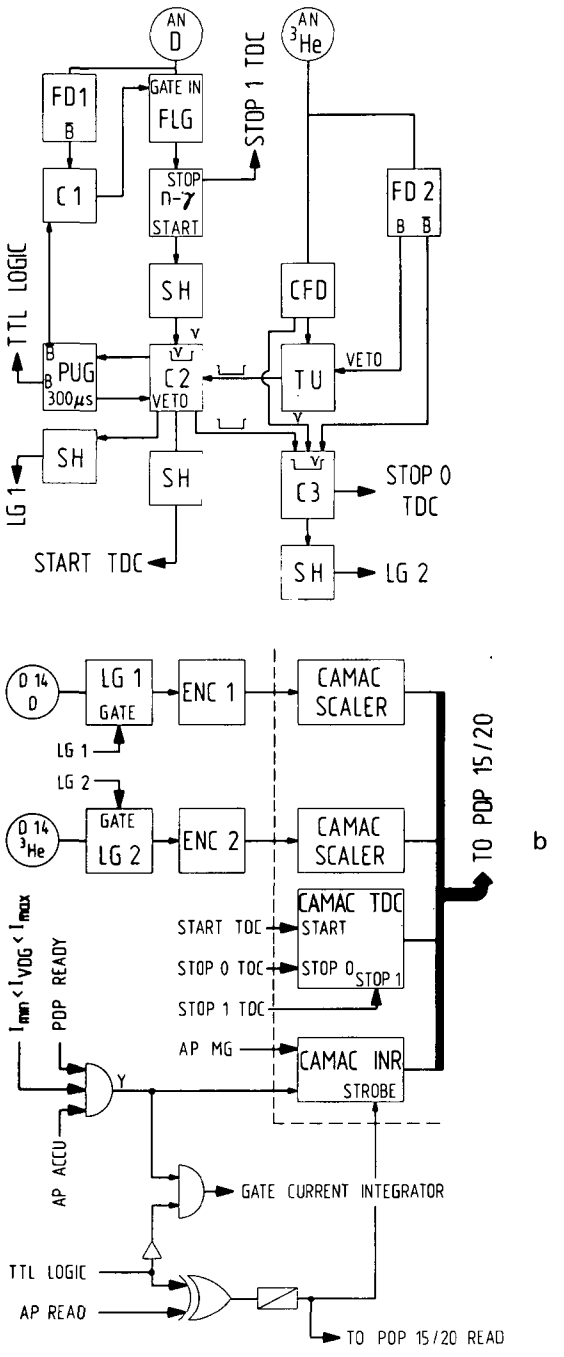

Fig. 2. Block diagram of the fast–slow electronics used with associated particle method. a) Fast section. AN-D, AN-He: anode of the photomultiplier (PM) connected to the scatterer and to the ^{3}He detector, respectively; FD1, FD2: fast discriminators; FLG: fast linear gate; C1–C3: fast coincidences; n–γ: neutron gamma discriminator[9]); CFD: constant fraction discriminator; SH: pulse shaper; PU: pile-up gate (constant dead time is typically 300 μs); TU: timing unit. b) Slow section. D14-D, D14-^{3}He: 14th dynode of the PM's; LG1, LG2: linear gate; ENC1, ENC2: encoder (direct-coupled analog to digital converter); TDC: time to digital converter (CAMAC); INR: input register (CAMAC); AP-ACCU: automatic programmer, function accumulation; AP-MG: automatic programmer, function "register on magnetic tape"; AP-READ: automatic programmer, function "read order to the PDP 15/20" (for clearing of all the CAMAC modules at the beginning of a run). $I_{min} < I_{VDG} < I_{max}$: accumulation of data is inhibited whenever the beam current is outside the range as defined by I_{min} and I_{max}.

with azeolith pellets. The dish was cooled down to below -140 °C by means of a copper rod plunging into a liquid N_2 reservoir outside the scattering chamber. No carbon deposit has ever been observed after weeks of running. The deuterium scatterer was a deuterated liquid scintillator NE-213 (Nuclear Enterprises, Edinburgh, U.K.). Three cylindrical scatterers of different dimensions have been used successively in order to check the importance of multiple scattering and edge effects, namely: 3×3 cm; 2×2 cm; 1×1 cm; (diameter$\times$height). Moreover a standard H-NE-213 cylindrical 2×2 cm scintillator has been used to check the data analysis method.

The geometry of the experiment was such that the aperture of the cone of detection for the ^{3}He was 1.5° which meant an aperture for the correlated neutron cone of 3°. Therefore the energy width of the incident neutrons was in the order of 0.07 MeV.

For the electronics, we have used a standard fast–slow time-of-flight spectrometer; in addition to this a n–gamma discrimination module[9]) was used. The block diagram is shown in fig. 2. The following parameters were recorded on a PDP 15/20 computer as an event: time-of-flight, pulse heights from the ^{3}He detector and the scatterer, pulse height from the TAC connected to the n–gamma module and finally some logical parameters. Fig. 3 shows a typical recoil energy spectrum.

3. Resolution and light output of the scatterer

A spectrum as shown in fig. 3 can be viewed as the result of the folding of a recoil energy spectrum ("pure spectrum") $g(x)$ with the resolution function (of the scintillator+electronics) $f(x, L)$ thus:

$$F(x) = \int_0^{x_m} g(x)\, f(x, L)\, \mathrm{d}L,$$

where $g(x)$ is in channel scale. It is well known that the relation between recoil energy and light output for such a scintillator is not a linear one,

except for electrons. We were therefore confronted to the problem of measuring the resolution $R(E_{recoil})$ on one hand and the light output $L(E_{recoil})$ on the other hand. In fact, if the resolution is known, $f(x, L)$ can be estimated reasonably well and with known fitting procedures[10,11]) one can get $g(x)$ from $F(x)$ provided that the experimental spectrum has been corrected for multiple scattering and edge effects. Then when $g(x)$ and $L(E)$ are determined one can calculate $g(E)$ and $g(\cos\theta_{CM})$ which is essentially the differential cross section in the center of mass. We have assumed that:

$$f(x,L) = \frac{1}{\sqrt{(2\pi)}}\frac{1}{\sigma(L)}\exp\left\{\frac{1}{2}\left(\frac{x-L}{\sigma(L)}\right)^2\right\},$$

x and L are in channel number and $\sigma^2(L)$ is the variance of the gaussian when centered at $x = L$.

When $g(x)$ is folded with a gaussian distribution $N(L, \sigma = \text{cst})$ the sharp edge of $g(x)$ is transformed into a smooth edge as shown in fig. 4. We shall now describe a method to determine X_m and σ from the measurements of $X_\sim$ and δ.

One can calculate that:

a) if $g(x) = \text{cst}$, $X_m = X_\sim$ and $\delta =$

$$\sqrt{\left(\frac{\pi}{2}\right)}\sigma = 1.253\sigma, \tag{1}$$

b) if $g(x) = ax$ and if $\sigma^2/X_\sim \ll 1$, $X_m \approx X_\sim - \sigma^2/X_\sim$

and:

$$\delta \approx 1.253\sigma\left\{1 + \left[\sqrt{\left(\frac{\pi}{2}\right)} - 2\sqrt{\left(\frac{2}{\pi}\right)}\right]\frac{\sigma}{X_m}\right\}$$

$$= 1.253\sigma \times \left(1 - 0.34\frac{\sigma}{X_m}\right). \tag{2}$$

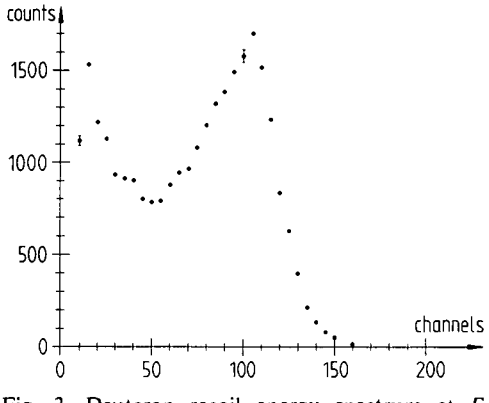

Fig. 3. Deuteron recoil energy spectrum at $E_n = 2.45$ MeV (without any correction for multiple scattering).

Let us define ε, R and ΔR as follows:

$$\varepsilon = \frac{X_\sim - X_m}{X_\sim}, \qquad R = \frac{\delta}{X_m}, \qquad \Delta R = R_0 - R,$$

$$\text{with } R_0 = 1.253\frac{\sigma}{X_m}. \tag{3}$$

Then one can see that: in case of a) $\varepsilon = 0$ and $\Delta R = 0$, and in case of b) $\varepsilon \approx (\sigma/X_\sim)^2$ and $\Delta R \approx 0.426\,(\sigma/X_m)^2$.

Tests by simulation on a computer have essentially verified these approximations and have moreover shown that if $g(x)$ is a polynomial of degree n a good approximation is given by:

$$\varepsilon = n\left(\frac{\sigma}{X_\sim}\right)^2, \qquad \Delta R = 0.426\,n\left(\frac{\sigma}{X_m}\right)^2. \tag{4}$$

$X_\sim$ and δ were obtained by fitting the simulated experimental spectrum by an orthogonal polynomial least square procedure[12]). These tests have also shown that as long as $(\sigma/X_\sim)^2 \leqslant 0.015$ and $n \leqslant 3$, eq. (4) is correct within 0.005 for ε and 0.001 for ΔR.

The situation described so far is of course unrealistic since σ has been kept constant. One knows[11]) that the experimental resolution R of a scintillation detector follows the law:

$$R^2 = A + B(L^{-1}), \tag{5}$$

where L is the light output or the pulse height given by the detector. From eqs. (1–5) one can see that the variance $\sigma^2(L)$ goes to zero when L goes to zero, as is expected. Similar tests by simulation have been conducted, but this time with realistic $\sigma(L)$. They have shown that reasonably good approximations are given by:

$$\varepsilon = \frac{n}{2}\left(\frac{\sigma}{X_\sim}\right)^2 \quad \text{and} \quad \Delta R = 0.426\frac{n}{2}\left(\frac{\sigma}{X_m}\right)^2. \tag{6}$$

They are correct within 0.005 for ε and 0.002 for ΔR when:

$(\sigma/X_\sim)^2 \leqslant 0.015$ and $n \leqslant 2$.

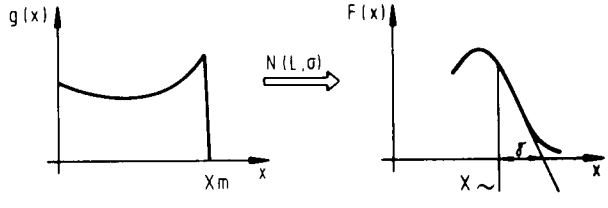

Fig. 4. A spectrum $g(x)$ folded by a gaussian resolution function $N(L, \sigma)$. X_m is the end point of $g(x)$, $X_\sim$ is the abscissa of the inflexion point of the right edge of $F(x)$ and δ is given by $\delta = F(X_\sim)/(-\mathrm{d}F/\mathrm{d}x|_{X_\sim})$.

These limitations are not very much restrictive since the first one means a resolution $R = 15\%$ (this is a value easily obtainable with a scintillation counter) and the second one will be satisfied in most cases by $g(x)$ in the vicinity of X_m (e.g. up to $3\times$standard deviation).

According to these findings, the following procedure has been used:

1) we have obtained recoil (e^- or d) energy spectra for as many incident energies as possible,
2) for each of these spectra we got $X_\sim$ and R as described in fig. 4 by fitting the right edge of the spectrum with a polynomial least square procedure[12]),
3) we have estimated X_m and $\sigma(X_m)$ from formula (1) and calculated $(\sigma/X_\sim)^2$ and $(\sigma/X_m)^2$. If the inspection of the experimental spectrum excluded $n = 0$, then $n = 1$ would be usually sufficient an approximation,
4) with the following formulas we computed X_m and R_0:

$$X_m = X_\sim - \frac{n}{2}\left(\frac{\sigma^2}{X_\sim}\right), \qquad R_0 = R + 0.426\frac{n}{2}(\sigma/X_m)^2, \tag{7}$$

5) we plotted R_0^2 as a function of $L(L = X_m)$ and made a least square fit to get A and B of the eq. (5),
6) by the formula

$$R_0(L = X_m) = 1.253\frac{\sigma(L = X_m)}{X_m} \quad \text{[eq. 3]}$$

we could write

$$\sigma^2(L) = \frac{A}{1.253^2}L^2 + \frac{B}{1.253^2}L, \tag{8}$$

7) we plotted X_m as a function of the recoil max energy (E_d) and fitted by a polynomial least square procedure* to get $L(E)$. The errors affecting the values of X_m and R_0 can be estimated from the above formula. In our case they have been approximated by:

$$\sigma^2_{X_m} = 0.25 + 25\times 10^{-6} X_\sim^2 \quad \text{and} \quad \sigma^2_{R_0} = X_m^{-2}.$$

4. Results

Fig. 5 shows the results of this procedure for the D-NE-213, 2×2 scintillator. The resolution which was determined by this method was consistent with the resolution obtained by means of a light emitting diode (LED). In this latter method, we have applied a LED (MLED 750) onto the wall of the scintillator cell in order to simulate as well as possible the real situation and to obtain a reasonable estimation of the coefficient A [eq. (5)]. The diode was excited by a fast pulser and the pulses from the photomultiplier were recorded by a multichannel analyser. By changing the excitation power, the light intensity from the LED could be modified. In this way, a few spectra (essentially of gaussian shape) could be recorded. Since the variance of a gaussian distribution is related in a simple way to its half width at half maximum, it was then easy to extract $\sigma(L)$ from these measurements.

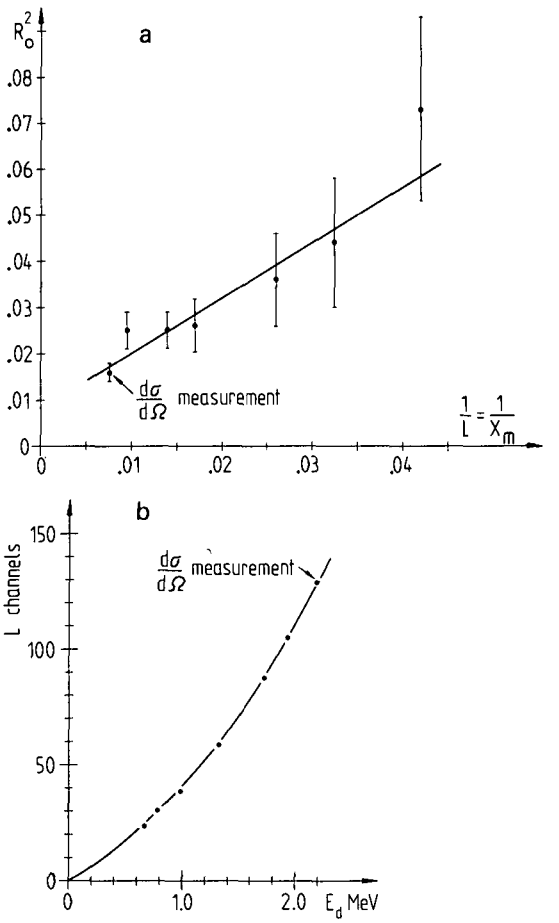

Fig. 5. a) The square of the resolution parameter R_0 as a function of $1/X_m$ for the D-NE-213, 2×2 cm scatterer. (The neutron source was the T (p, n) ^{3}He reaction except for the $d\sigma/d\Omega$ experiment). ● Experimental results, — result of a least square fit. b) Light output for the same scatterer as a function of deuteron energy. ● experimental results, — result of a least square fit. Error bars on the experimental values of L are smaller than the plotted points; they include the uncertainty of 30 keV in the deuteron energy.

* It was not necessary to fit the data $L(E_d)$ with a Birks formula since the data $L(E_d)$ covered the useful energy range of the measured energy spectra; however we have forced the fit to go through zero for $L = 0$.

A complete description of the method used to extract $g(\cos\theta_{CM})$ from $F(x)$ will be published in a later paper. Our preliminary results are the following: At 2.45 MeV, our measured cross-section fits very well with the BNL 400 data from $\cos\theta_{CM} = 0.3$ (our experimental limit at forward angle) to $\cos\theta_{CM} = -0.8$ but shows a more pronounced peaking from -0.8 to -1.0. A fit with Legendre polynomials indicate that a development up to P_6 is necessary. Therefore the highest partial wave should be increased to $l = 3$.

The authors express their appreciation to the computer centers of the University of Neuchâtel and of EPF-Lausanne for giving them the opportunity of many necessary hours of computer-time.

References

1) S. Jaccard, J. Piffaretti, R. Viennet and J. Weber, Proc. Third Intern. Symp. on *Polarization phenomena in nuclear reaction*, Madison (1970) p. 448.

2) D. Bovet, P. Chatelain, S. Jaccard, Y. Onel, J. Piffaretti, R. Viennet and J. Weber, Proc. Int. Conf. on *The interaction of neutrons with nuclei*, Lowell (1976) p. 1357.

3) J. D. Seagrave and L. Cranberg, Phys. Rev. **105** (1957) 1816.

4) M. Brüllman, H.-J. Gerber and D. Meier, Helv. Phys. Acta **31** (1958) 318.

5) M. Brüllmann, H.-J. Gerber, D. Meier and P. Scherrer, Helv. Phys. Acta **32** (1959) 511.

6) J. H. Coon and H. H. Barshall, Phys. Rev. **70** (1946) 592.

7) M. D. Goldberg, V. M. May and J. R. Stehn, BNL-400, vol. 1 (1962).

8) H. B. Willard, J. K. Bair and C. M. Jones, Phys. Lett. **9** (1964) 339.

9) P. Betz, G. Braun, G. Hammel and J. Urban, Nucl. Instr. and Meth. **119** (1974) 199.

10) V. Morgan and R. L. Walter, Phys. Rev. **168** (1968) 1114.

11) D. Blanc, F. Cambou et G. Vedrenne, Journal de Physique suppl. **27** (1966) C1-71.

12) D. J. Hudson, Statistics Lectures II, CERN-64-18 (1964); P. R. Bevington, *Data reduction and error analysis for the physical sciences*, (MacGraw-Hill, New York, 1969).

1.B: 2.B

Nuclear Physics **A319** (1979) 71 – 88;

THE (n, d) ELASTIC DIFFERENTIAL CROSS SECTION AT E = 2.48 AND 3.28 MeV †

P. CHATELAIN ††, Y. ONEL ††† and J. WEBER

Institut de Physique de l'Université, Rue A.-L. Breguet 1, CH-2000 Neuchâtel, Switzerland

Received 13 November 1978

Abstract: We have measured the (n, d) elastic differential cross section at incident neutron energies of 2.48 and 3.28 MeV. We have used the recoil energy spectrum method. Tables of measured cross sections are presented. Fits with Legendre polynomials confirm that partial waves up to $l = 3$ and 5 should be present in the phase shift analyses of this reaction at 2.48 and 3.28 MeV respectively. We compare our results with theoretical predictions. Good agreement with Alt's calculations at 3.28 MeV is observed.

E NUCLEAR REACTIONS ^{2}H(n, n), E = 2.48, 3.28 MeV; measured $\sigma(E, \theta)$.

1. Introduction

The number of available elastic (n, d) differential cross section data at low energies [1]) is very limited; therefore it is difficult to perform a statistically clear test for the polynomial P_3 or higher when the Legendre polynomials are used for fitting the data. This situation precludes the introduction of partial waves with $l = 3$ or higher in the parametrization of the phase shift analysis unless one includes them by a model dependent calculation [2, 3]). In this respect, the situation is much more favourable in the (p, d) case [4]). In order to be able to introduce in a model independent way partial waves up to $l = 3$ or higher for our study of the (n, d) elastic interaction [5 – 7]), we have measured the (n, d) elastic differential cross section with special emphasis on the large angle range. The measurements were done near the energies of 2.45 and 3.27 MeV, since a few data already exist at these two energies [1]) which could be used for the purpose of normalization and comparison, and since an angular distribution of the neutron depolarization factor $D(\theta)$ ($30° \leqq \theta_{c.m.} \leqq 120°$) at 2.45 MeV incident energy is currently being measured in our laboratory [a few results have already been published in ref. [7])]. Another interesting outcome of these

† Work supported in part by the Swiss National Science Foundation.
†† This article includes parts of the thesis of P. Chatelain.
††† Present address: Université de Genève, Département de Physique nucléaire et corpusculaire, Bd d'Yvoy 32, CH-1211 Genève 4, Switzerland.

new measurements was to compare them with the three-body calculations done with realistic potentials [8]).

2. Experimental arrangement

We have used the recoil-energy-spectrum method [e.g. ref. [9])] because of its advantages, namely: the cross section can be measured in a large angular range in one experiment and this angular range extends up to 180° which it does not with other methods. A detailed description of our experimental set-up has already been published in ref. [10]). The relevant geometrical parameters for our experiments are listed in table 1. It should be noted that we have used three scatterers of different dimensions in order to be able to check the validity of our procedure for multiple scattering correction and to observe possible edge effects.

TABLE 1.

The kinematical parameters of the experimental set-up

E_d (MeV) (beam)	θ_1 [a]) (deg)	θ_2 [a]) (deg)	E_n (MeV)	Scatterer D-NE-213		Distance from target to ^{3}He beam collimator (cm)	Distance from target to D-NE-213 (cm)
				diam. (cm)	height (cm)		
2.18	29.6	109.6	2.44±0.03 [b])	1	1	13.6	26.5
2.18	30.6	107.9	2.48±0.03 [b])	2	2	13.6	44.5
2.18	29.3	110.0	2.43±0.03 [b])	3	3	13.6	66.5
2.23	45.0	81.0	3.28±0.03 [b])	1	1	13.6	32.4

[a]) θ_1 and θ_2 are the angles of emission of the ^{3}He and neutron beams respectively [10]).

[b]) This value of 30 keV includes the uncertainty in the deuteron incident energy and the neutron energy spread associated with the solid angle of detection of the ^{3}He beam.

The position of the scatterer-scintillator D1 [see fig. 1, ref. [10])] could be remotely moved in two directions perpendicular to the neutron beam. Therefore the cross section of this neutron beam – as defined by the ^{3}He beam collimator – could be measured; it was then possible to fix the position of the scatterer so that the neutron beam would be distributed evenly over it.

Each one of the four experiments listed in table 1 consisted of more than 100 runs of about one hour each so that the stability of each part of the electronics, as well as the overall stability of each run, could be regularly checked.

3. Data analysis

Firstly, the experimental spectrum (expressed as the number of counts per channel x) had to be corrected for background and, secondly, for neutron multiple

scatterings in the scatterer-scintillator. Then we had to take care of problems due to the finite resolution of the detection device and to the non-linear relationship between the deuteron recoil energy and the light yield of the scatterer-scintillator. Regarding the finite resolution, we followed the method described in ref. [9]) that is: we essentially fitted to the experimental spectrum a polynomial $g(x) = a_0 + a_1 x + \ldots + a_n x^n$ (x in channel units) folded with a resolution function. Through this method, a set of discrete experimental data was transformed into the knowledge of the coefficients of the fitted polynomial. Since we were not aware of any method allowing the direct extraction of the phase shifts from these coefficients [except in the simple case of the $\frac{1}{2}+0 \rightarrow \frac{1}{2}+0$ reaction [11])], we have used a procedure which resulted in a set of discrete values of the cross section which could then be used easily in connection with other sets in a phase shift analysis. As a summary, the complete sequence of the data analysis steps was as follows:

(i) Background correction.

(ii) Multiple scattering correction.

(iii) Point to point transformation of $g(x_i)$ into $g(E_d^{(i)}$ recoil) and then into $g(\cos\theta_{c.m.}^{(i)})$ through the relationships $E_d(x)$ and $\cos\theta_{c.m.}(E_d)$ (x_i = ith channel in the fitting range, $i = 1 \ldots N$).

(iv) Normalization of $g(\cos\theta_{c.m.}^{(i)})$ to get $(d\sigma/d\Omega)(\cos\theta_{c.m.}^{(i)})$.

(v) Constitution of a set of N discrete values of the cross section based on the N normalized values of $g(\cos\theta_{c.m.}^{(i)})$, so that this set had a meaningful statistical content.

We shall now describe in more details steps (i) to (v).

3.1. BACKGROUND CORRECTION

Among others, the following parameters were recorded on magnetic tape [10]): energy spectra from the ^{3}He detector and from the D-NE-213 scatterer-scintillator (D1), the time-of-flight (TOF) spectrum as defined by these two detectors and finally, the n-γ discrimination spectrum.

To allow us to perform the preliminary background subtraction and construct a corrected matrix correlating the TOF and scatterer spectrum, realistic acceptance windows were set upon the ^{3}He and n-γ discrimination spectra. The scatterer spectrum was then further corrected for any left over background through careful inspection and treatment of this matrix. On the other hand, it was verified that the n-γ discrimination did not cause any distortion in the first usable channels of the scatterer spectrum. The correction for the proton contamination in our D-NE-213 scintillators was considered to be negligible. Indeed, by taking into account that $n_H/n_D = 1\,\%$ (according to the manufacturer), that the light yields due to proton and deuteron recoils were in the ratio $L_p/L_D \approx 2$, then the n-p scattering contribution in each channel was estimated to be of the order of 0.5 %. The

contributions to the spectrum from the scintillator cell walls were also estimated to be negligible.

3.2. MULTIPLE SCATTERING CORRECTION

The probability of neutron multiple scatterings in the scatterer could not be neglected, in the present energy range, even in the case of the smallest of our scatterer (1×1 cm^2). The contribution of multiple scattering to the recoil spectrum could be as high as 14 to 34 % depending on the size of the scatterer, the incident neutron energy and the spectrum channel. We have used a Monte Carlo code [5, 12]) to compute a correction factor for each spectrum channel of each experiment listed in table 1. This factor was obtained by the following procedure: firstly, the recoil energy spectra for the simple and total (simple + multiple) scattering events were computed by the Monte Carlo code. Secondly, these spectra were folded with a resolution function as given by eq. (2) of subsect. 3.3. Finally, the ratio of the number of simple events to the number of total events for each channel of the folded spectra was computed and used as a correction factor.

Fig. 1 shows one set of these spectra compared with the corresponding experimental spectrum. The agreement between the total spectrum and the experimental spectrum is good. Nevertheless, in order to increase the degree of coincidence in our method of correcting for the multiple scattering, we have measured the scattering cross section at a nominal energy of 2.45 MeV with three scatterers different from each other by their dimensions (listed in table 1).

Since these three differential scattering cross sections coincided within the experimental errors, our correcting method for the multiple scattering could be considered as adequate.

No edge effect has been observed. This was expected since simple estimation had showed that this type of effect should be very small even for the smallest of our scatterers.

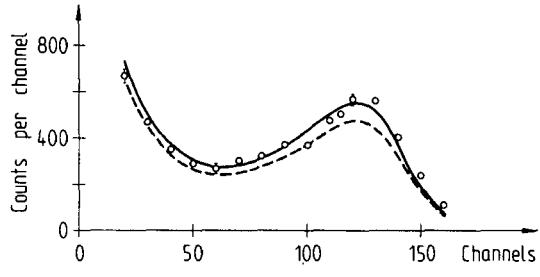

Fig. 1. Recoil energy spectra computed by the Monte Carlo method. Incident energy E = 2.44 MeV; scatterer-scintillator, D-NE-213, 1×1 cm^2; solid line, "total" spectrum folded with the relevant resolution function $f(x, L)$; dashed line, "simple" spectrum folded with the relevant resolution function $f(x, L)$. ("Total" and "simple" are defined in the text.) Open circles are a sample of the experimental spectrum.

3.3. TRANSFORMATION OF THE EXPERIMENTAL SPECTRUM INTO A DISCRETE SPECTRUM AS A FUNCTION OF $\cos(\theta_{c.m.})$

At this point, the experimental spectrum could be considered as a sample of the function $F(x)$ which is itself the result of the folding of a function $g(L)$ by a resolution function $f(x, L)$ of the scintillator and its associated electronics [10]), so that

$$F(x) = \int_0^{X_m} g(L) f(x, L) \mathrm{d}L, \tag{1}$$

where x and L are in channel units, X_m is the end channel of $g(x)$ [ref. [10])], and where $f(x, L)$ was assumed to be

$$f(x, L) = \frac{1}{\sqrt{2\pi}\sigma(L)} \exp\left\{-\tfrac{1}{2}\left(\frac{x-L}{\sigma(L)}\right)^2\right\}. \tag{2}$$

Moreover, following the argument of ref. [9]), we then defined $g(x)$ to be

$$g(x) = a_0 + a_1 x + a_2 x^2 + \ldots + a_n x^n. \tag{3}$$

With eqs. (1) and (3), one gets

$$F(x) = \sum_{j=0}^{n} a_j G_j(x), \tag{4}$$

where

$$G_j(x) = \int_0^{X_m} L^j f(x, L) \mathrm{d}L.$$

In eq. (2), $\sigma^2(L)$ can be written as [10])

$$\sigma^2(L) = R_v^2 L^2 + R_E^2 L. \tag{5}$$

Typical values of R_v^2 and R_E^2 which were used in our analyses are listed in table 2; the method that we have used to measure these coefficients is described in detail in ref. [10]).

While fitting $F(x)$ to the experimental spectrum, searches were made to verify that the values of the parameters X_m [end point of spectrum $g(x)$], R_v^2 and R_E^2 [as obtained by the method described in ref. [10])], would indeed produce a minimum of the reduced χ^2.

The function $F(x)$ was fitted to the experimental data in the channel range defined by a lower limit X_{min} (essentially defined by the electronics) and by an upper limit X_{max} (close to or equal to X_m). It was observed that fits with slightly different values of X_{max} would lead to functions $g(x)$ that would differ slightly

TABLE 2

Typical values of the parameters R_v^2 and R_E^2 (eq. (5)) and b_1 and b_2 (eq. (6))

E_n (MeV)	D-NE-213 diam. × height (cm²)	$R_v^2 \pm \sigma_{R_v^2}$	$R_E^2 \pm \sigma_{R_E^2}$ (channel)	$b_1 \pm \sigma_{b_1}$ (channel/MeV)	$b_2 \pm \sigma_{b_2}$ (channel/(MeV)²)
2.48	2×2	$(4.97 \pm 1.72) \times 10^{-3}$	0.764 ± 0.146	24.92 ± 1.05	15.19 ± 0.68
3.28	1×1	$(7.8 \pm 1.1) \times 10^{-3}$	0.440 ± 0.088	19.27 ± 0.84	9.43 ± 0.40

from one another in the channel region corresponding to scattering angles near 180°. By folding $g(x)$ with the resolution function (eq. (2)), we could compare each solution with the experimental spectrum through a χ^2 procedure. It turned out that when X_{max} was alowed to vary within ± 5 channels around X_m, the solutions that we obtained for $g(x)$ were equivalent from a statistical point of view. This point will be discussed further in subsect. 3.5. Fig. 2 shows an example of $F(x)$ (eq. (4)) compared with the experimental spectrum and fig. 3 shows the corresponding function $g(x)$ and the folded $g(x)$ function compared with the same experimental spectrum.

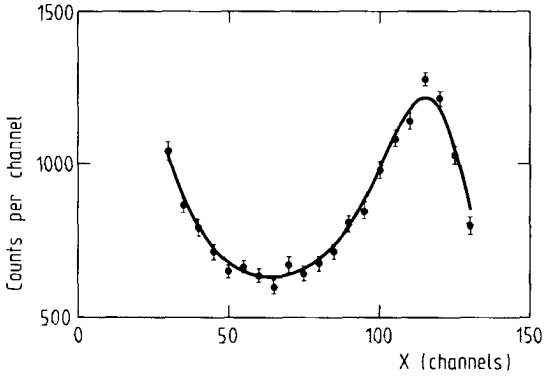

Fig. 2. The solid line gives $F(x)$ (eq. (4)) fitted to the experimental spectrum between $X_{min} = 30$ and $X_{max} = 130$. (Reduced $\chi^2 = 1.4$.) Solid circles are a sample of the experimental spectrum (corrected for background and multiple scattering). Incident neutron energy $E = 2.48$ MeV; scatterer-scintillator D-NE-213, 2×2 cm².

It is well known that, for scintillators such as those which we have used in this experiment, the relationship between deuteron energy and light output is not linear. It could be described as [10])

$$L(E_d) = b_1 E_d + b_2 E_d^2, \tag{6}$$

with L in channel units and E_d in MeV. Typical values of b_1 and b_2 are listed in

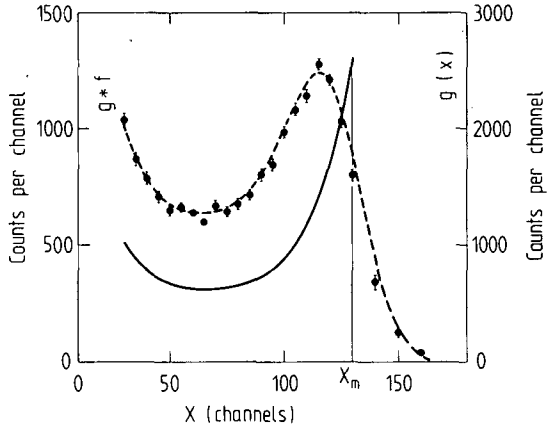

Fig. 3. The solid line gives $g(x)$ (eq. (3)) as obtained from the fit of $F(x)$ to the experimental spectrum (see fig. 2); the dashed line gives the folded function $g(x)$; and the solid circles are a sample of the experimental spectrum.

table 2. Since the Jacobian which transforms $g(x)$ into $g(E_d)$ includes the derivative of eq. (6), the precise measurement of b_1 and b_2 was of great importance regarding the shape of $g(E_d)$ and consequently of the cross section. Therefore we devised the procedure described in ref. [10]) to measure $L(E_d)$ accurately and in a reproducible manner. We are confident that our method gives reliable results for the following reasons: the experimental set-up was used without modification throughout the measurements of the cross sections and of the relevant light yield $L(E_d)$; the inflexion point of the right edge of the recoil spectrum was connected in a known way to the end point X_m of the spectrum $g(x)$ and finally the errors could be computed in a reliable way. From the knowledge of the precise value of b_1 and b_2, it was then a simple matter to compute $g(E_d^{(i)}(x_i))$ where $i = 1 \ldots N$. The transformation of $g(E_d^{(i)})$ into $g(\cos\theta_{c.m.}^{(i)})$ is straightforward and need not be described.

3.4. NORMALIZATION

Since our experimental set-up was not devised to produce absolute cross sections, we have normalized our angular distributions $g(\cos\theta_{c.m.}^{(i)})$ to the values given in ref. [1]) for $\cos\theta_{c.m.} = 0$, specifically 115 and 100 mb/sr at 2.45 and 3.27 MeV, respectively. The possible normalization to the total cross section is discussed in sect. 4. These N normalized values can be considered as forming a set of N smoothed values of the cross section.

3.5. SYSTEMATIC ERROR

We mentioned in subsect. 3.3 that by changing the upper limit by a few channels in the fitting procedure we got somewhat different results for $g(x_i)$, and conse-

quently for $d\sigma(\cos\theta^{(i)}_{c.m.})/d\Omega$, in the region of large scattering angles. Fig. 4 shows an example of this behaviour. Since each of these solutions was statistically equivalent, we took point by point, the mean value of the three solutions for $d\sigma(\cos\theta^{(i)}_{c.m.})/d\Omega$ which were obtained by fitting $F(x)$ to the experimental spectrum up to X_m-5, X_m, X_m+5 channels respectively. Hence we go a set of N smoothed data which we then used as a starting point for the creation of the N scattered data set (see subsect. 3.6).

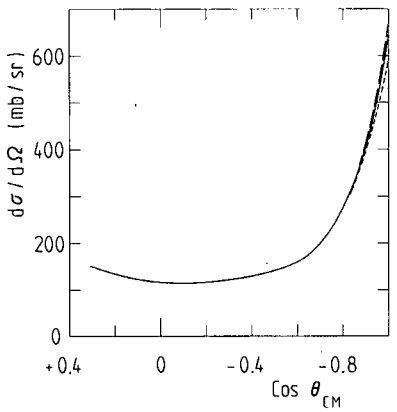

Fig. 4. The (n, d) cross section at large scattering angle. Dependence on the channel X_{max} is defined as the upper limit of the range of fitting. The solid line is for $X_{max} = X_m$; the long-dashed line, $X_{max} = X_m-5$; and the short-dashed line $X_{max} = X_m+5$. Energy $E = 2.48$ MeV; scatterer-scintillator, D-NE-213, 2×2 vm^2.

The corresponding systematic uncertainty (labeled SD_{fit} in tables 3 and 4) was then estimated by the following procedure. Since any solution for $d\sigma(\cos\theta^{(i)}_{c.m.})/d\Omega$ had the same statistical weight in the range

$$\Delta_i = \left(\frac{d\sigma}{d\Omega}\right)_i (X_m-5) - \left(\frac{d\sigma}{d\Omega}\right)_i (X_m+5),$$

$SD^{(i)}_{fit}$ was assumed to be well estimated by the variance of a uniform distribution over the range Δ_i:

$$SD^{(i)}_{fit} = \sqrt{\frac{1}{12}\Delta_i^2}.$$

The statistical standard deviations $SD^{(i)}_{stat}$ (subsect. 3.6) and $SD^{(i)}_{fit}$ were then combined through the known statistical formula to estimate the total uncertainty $SD^{(i)}_{tot}$.

3.6. CREATION OF A SET OF N DISCRETE AND UNSMOOTHED VALUES OF THE CROSS SECTION

As we said earlier, our data reduction technique produced, for each experiment listed in table 1, a set of coefficients a_j (eq. (4)). Since we did not know of any method of determining the phase shifts from these coefficients, it was decided to extract from our results a set of discrete, statistically meaningful, values of the cross section. This procedure would have the advantage that this set could be easily associated to other already published sets of data, for example the data at small scattering angles [1]), to be used as input data to Legendre polynomials fits or phase shift analyses. This new set of data had to fulfil some statistical conditions which we defined as follows:

(a) The new data should not be smoothed but rather scattered in a convenient way so as to preserve, in further fits, the usual statistical interpretation of the minimum χ^2.

(b) A fit of polynomials to the new data should produce the same coefficients (within the error range) as the ones of the polynomial from which these data were extracted.

(c) The covariance matrices of these two sets of coefficients should be equivalent.

It is shown in the appendix that these three conditions could be fulfilled by the following procedure.

To each one of the N smoothed values of the cross section a standard deviation σ_i was associated (labeled SD_{stat} in tables 3 and 4), which would depend on $(d\sigma/d\Omega)_i$, the normalization factor and the width of the bin centered at $\cos\theta_{c.m.}^{(i)}$. Thus the coherence was insured between the σ and the standard deviations related to the experimental spectrum. Then a new value of the cross section was extracted at each point i by random sampling according to a Gaussian density function $N((d\sigma/d\Omega)_i, \sigma_i)$.

4. Results

4.1. $E = 2.48$ MeV

The results that we obtained with the three scatterers listed in table 1 were equivalent. Therefore, our correcting method for multiple scattering effects and for analysing the data could be considered as adequate. (Another check was provided by an experiment with a hydrogen-NE-213 scatterer. The data analysis produced a uniform differential cross section as was expected.) For $\cos\theta_{c.m.} \leqq 0.305$, we present the results obtained with the 2×2 cm^2 scatterer and for $0.310 \leqq \cos\theta_{c.m.} \leqq 0.493$, the results obtained with the 1×1 cm^2 scatterer (in the latter experiment the electronics threshold could be set somewhat lower). Fig. 5 depicts the behaviour of the final smoothed data set with the relevant confidence limits. Table 3 lists

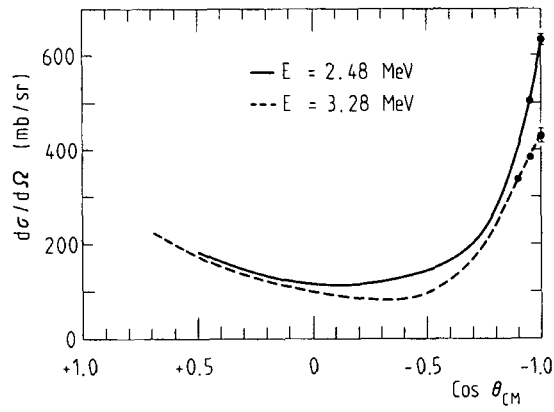

Fig. 5. Trends of the final smoothed data sets. A few data points are plotted so as to indicate the confidence limits defined by their error bars (when not shown, they are smaller than the dots).

the unsmoothed data set. Fig. 6 shows a sample of this set together with the differential cross section given in ref. [1]).

In order to gain some information on the maximum order of the partial wave in the scattering amplitude that would be statistically significant, we fitted our results (listed in table 3) together with Seagrave's values for $\cos\theta_{c.m.} > 0.5$ at $E = 2.45$ MeV [ref. [13])] with Legendre polynomials. The usual technique [14]) and the stepwise regression [15]) were used. Both methods showed that the data were statistically correctly (reduced $\chi^2 \approx 0.8$) fitted by

$$\frac{d\sigma}{d\Omega}(\cos\theta_{c.m.}) = \sum_{j=0}^{6} c_j P_j(\cos\theta_{c.m.})$$

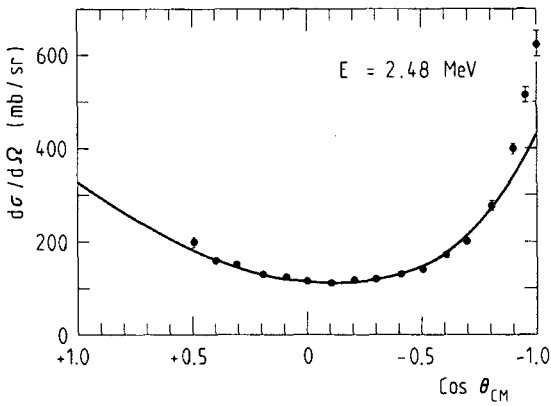

Fig. 6. The (n, d) elastic differential cross section. Incident neutron energy is 2.48 MeV; the solid circles are a sample of the present results (unsmoothed data set). The error bars are equal to SD_{tot} (subsect. 3.5). The solid line is the trend of $d\sigma/d\Omega$ as depicted in ref. [1]).

[the F_{1,ν_2} (5 %) test was used to fix the limit of the expansion]. The integration of $d\sigma/d\Omega$ over $\cos\theta_{c.m.}$ gave a total cross section of 2450 ± 15 mb. This result could be compared to known values of σ_t for further normalization [for example 2395 ± 36 mb from ref. [16]), see also ref. [17])].

4.2. $E = 3.28$ MeV

The behaviour of the final smoothed data set is shown in fig. 5. Table 4 lists our results (unsmoothed data set) a sample of which is displayed in fig. 7. These data have been fitted [14, 15]), together with Seagrave's results [13]) at 3.27 MeV for $\cos\theta_{c.m.} > 0.7$ with Legendre polynomials (reduced $\chi^2 \approx 0.8$). These fits showed that polynomials of order as high as nine were statistically significant.

Integration of $d\sigma/d\Omega$ over $\cos\theta_{c.m.}$ gave a total cross section of 2145 ± 13 mb as compared to 2140 ± 35 mb [ref. [16])].

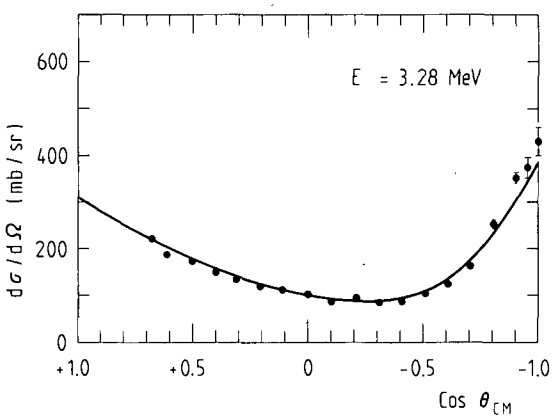

Fig. 7. The (n, d) elastic differential cross section. Incident neutron energy is 3.28 MeV; the solid circles are a sample of the present results (unsmoothed data set); the error bars are equal to SD_{tot} (subsect. 3.5); and the solid line is the trend of $d\sigma/d\Omega$ as depicted in ref. [1]).

5. Comparison with theoretical predictions

In this section, we compare our data with the results obtained by Alt and Bakker [8]) at 2.45 and 3.27 MeV, Fuda and collaborators [18, 19]) at 2.45 MeV, and Fayard and Lamot [20]) at 2.6 MeV.

Alt and Bakker have calculated three-nucleon observables below the break-up threshold by using a unitary pole approximation (UPA) [21]) to the soft-core Malfliet-Tjon potentials MT I and MT III. The triton energy E_t and the doublet scattering length that they have obtained are in good agreement with the results of other authors. Two advantages of their method are a tremendous simplification of the three-body equations and the inclusion in their rank-one potential, through

TABLE

The 2.48 MeV (n, d)

$\cos\theta_{c.m.}$	$d\sigma/d\Omega$	SD_{stat}	SD_{fit}	SD_{tot}	$\cos\theta_{c.m.}$	$d\sigma/d\Omega$	SD_{stat}	SD_{fit}	SD_{tot}
0.493	199.3	7.9	0.0	7.9	0.474	189.5	7.8	0.0	7.8
0.417	170.7	7.6	0.0	7.6	0.399	160.1	7.6	0.0	7.6
0.345	153.6	7.3	0.0	7.3	0.327	149.7	7.3	0.0	7.3
0.286	147.6	4.5	0.0	4.5	0.268	147.7	4.5	0.0	4.5
0.214	131.4	4.4	0.0	4.4	0.196	130.9	4.4	0.0	4.4
0.145	126.5	4.3	0.0	4.3	0.128	125.5	4.3	0.0	4.3
0.078	119.6	4.4	0.0	4.4	0.062	126.8	4.3	0.0	4.3
0.014	123.6	4.4	0.0	4.4	−0.001	117.2	4.4	0.0	4.4
−0.047	116.5	4.4	0.0	4.4	−0.062	104.9	4.4	0.0	4.4
−0.106	110.8	4.5	0.0	4.5	−0.121	111.7	4.4	0.0	4.4
−0.164	110.7	4.6	0.0	4.6	−0.178	119.9	4.6	0.0	4.6
−0.220	116.3	4.6	0.0	4.6	−0.234	110.8	4.6	0.0	4.6
−0.275	118.1	4.7	0.0	4.7	−0.288	121.0	4.8	0.0	4.8
−0.328	120.7	4.9	0.0	4.9	−0.341	117.6	4.9	0.0	4.9
−0.379	124.0	5.1	0.0	5.1	−0.392	129.9	5.0	0.0	5.0
−0.430	128.2	5.2	0.0	5.2	−0.442	133.2	5.2	0.0	5.2
−0.479	144.2	5.4	0.0	5.4	−0.491	148.4	5.4	0.0	5.4
−0.527	145.8	5.6	0.0	5.6	−0.539	149.0	5.6	0.0	5.6
−0.575	154.8	5.9	0.0	5.9	−0.586	157.3	5.9	0.0	5.9
−0.621	172.8	6.1	0.0	6.1	−0.632	174.7	6.2	0.0	6.2
−0.666	195.4	6.6	0.0	6.6	−0.677	196.5	6.5	0.0	6.5
−0.711	202.8	6.8	0.0	6.8	−0.722	210.3	7.0	0.0	7.0
−0.754	244.3	7.6	0.0	7.6	−0.765	244.4	7.5	0.0	7.5
−0.797	263.4	8.1	0.0	8.1	−0.808	279.4	8.1	0.0	8.1
−0.840	324.7	8.8	1.4	8.9	−0.850	331.3	8.9	2.0	9.2
−0.881	371.3	9.5	4.3	10.5	−0.892	389.0	9.7	5.2	11.0
−0.922	448.7	9.9	8.4	13.0	−0.935	457.5	10.6	9.5	14.2
−0.963	522.2	11.6	14.2	18.4	−0.973	554.6	11.9	15.6	19.6
−1.000	624.4	13.8	21.7	25.7					

[a]) SD_{stat}, SD_{fit} and SD_{tot} are defined in subsect. 3.5. Both SD and $d\sigma/d\Omega$ are given in mb/sr.

the peculiar form factors, of a good part of the repulsion contained in the potentials MT I and MT III [this repulsion has the effect of increasing the differential cross section in the forward and backward directions, improving the agreement with experimental results [8, 22])].

Fuda and co-workers have used an on-shell theory with a separable potential model for the $^3S_1$ and $^1S_0$ two-nucleon amplitudes to calculate the $^{2,4}\delta_{1,2,3}$ phase shifts and the N/D equations of Barton and Phillips to calculate $k\cot^2\delta_0$ (in the computation of the cross section, we have assumed $^4\delta_0$ to be $-65.6°$ which is in the range of commonly accepted values).

Fayard and Lamot have used the following interactions: for the $^1S_0$ wave, the M5 parametrization; for the $^3S_1$-$^3D_1$ waves, the ACS4 ($P_D = 4\,\%$) parametrization;

3

elastic cross section [a])

$\cos\theta_{c.m.}$	$d\sigma/d\Omega$	SD_{stat}	SD_{fit}	SD_{tot}	$\cos\theta_{c.m.}$	$d\sigma/d\Omega$	SD_{stat}	SD_{fit}	SD_{tot}
0.454	189.3	7.7	0.0	7.7	0.436	159.8	7.7	0.0	7.7
0.381	158.9	7.5	0.0	7.5	0.363	151.7	7.4	0.0	7.4
0.310	147.3	7.2	0.0	7.2	0.305	153.1	4.5	0.0	4.5
0.250	130.9	4.4	0.0	4.4	0.231	137.3	4.4	0.0	4.4
0.179	127.0	4.4	0.0	4.4	0.162	128.5	4.4	0.0	4.4
0.111	121.2	4.3	0.0	4.3	0.094	126.4	4.3	0.0	4.3
0.046	117.6	4.3	0.0	4.3	0.030	118.0	4.3	0.0	4.3
−0.017	107.3	4.4	0.0	4.4	−0.032	107.0	4.4	0.0	4.4
−0.077	116.2	4.4	0.0	4.4	−0.092	115.3	4.5	0.0	4.5
−0.136	109.0	4.5	0.0	4.5	−0.150	111.6	4.6	0.0	4.6
−0.192	116.2	4.6	0.0	4.6	−0.206	118.1	4.6	0.0	4.6
−0.248	120.1	4.7	0.0	4.7	−0.261	116.3	4.7	0.0	4.7
−0.301	119.9	4.8	0.0	4.8	−0.315	124.6	4.8	0.0	4.8
−0.354	120.4	4.9	0.0	4.9	−0.367	114.1	5.0	0.0	5.0
−0.405	131.8	5.1	0.0	5.1	−0.417	134.6	5.1	0.0	5.1
−0.455	128.7	5.2	0.0	5.2	−0.467	141.2	5.4	0.0	5.4
−0.503	142.8	5.5	0.0	5.5	−0.515	138.2	5.5	0.0	5.5
−0.551	153.3	5.6	0.0	5.6	−0.563	147.8	5.7	0.0	5.7
−0.598	155.1	6.0	0.0	6.0	−0.609	172.3	6.0	0.0	6.0
−0.644	171.7	6.3	0.0	6.3	−0.655	176.2	6.5	0.0	6.5
−0.689	192.7	6.7	0.0	6.7	−0.699	203.7	6.8	0.0	6.8
−0.733	212.5	7.1	0.0	7.1	−0.744	223.5	7.4	0.0	7.4
−0.776	246.3	7.6	0.0	7.6	−0.787	265.7	8.0	0.0	8.0
−0.819	297.7	8.4	0.0	8.4	−0.829	310.0	8.6	1.2	8.7
−0.861	343.4	9.1	2.6	9.5	−0.871	356.1	9.6	3.5	10.2
−0.902	399.2	10.2	6.1	11.9	−0.912	412.1	10.4	7.2	12.7
−0.943	479.2	11.7	11.0	16.1	−0.953	516.2	11.4	12.4	16.8
−0.983	591.2	12.5	17.9	21.8	−0.992	579.5	13.5	19.9	24.0

and for the $^1P_1$, $^3P_0$, $^3P_1$ and $^3P_2$ waves, the Graz potentials. They have made "exact" calculations throughout.

The results of these calculations are shown in fig. 8 together with some of our data points at 2.48 MeV. For comparison purposes, Seagrave's measurements [13]) are also shown as well as the trend ("BNL trend") of the cross section as depicted in ref. [1]). It can be seen that each calculated cross section lies below the "BNL trend" at small scattering angles and below our measurements in the backward direction. Hence, one can conjecture [see for example fig. 6 of ref. [8])] that if a better agreement could have been obtained in the forward direction between the calculations and "BNL trend", then these calculations would have shown a more pronounced peaking at large angles. Hence a better agreement with our data would have been observed.

TABLE

The 3.28 MeV (n, d)

$\cos\theta_{c.m.}$	$d\sigma/d\Omega$	SD_{stat}	SD_{fit}	SD_{tot}	$\cos\theta_{c.m.}$	$d\sigma/d\Omega$	SD_{stat}	SD_{fit}	SD_{tot}
0.681	223.9	5.8	0.0	5.8	0.657	214.7	5.8	0.0	5.8
0.587	194.3	5.7	0.0	5.7	0.565	184.2	5.7	0.0	5.7
0.501	172.7	5.5	0.0	5.5	0.480	167.6	5.5	0.0	5.5
0.421	159.7	5.4	0.0	5.4	0.401	148.7	5.3	0.0	5.3
0.345	139.4	5.4	0.0	5.4	0.327	143.8	5.2	0.0	5.2
0.273	117.4	5.2	0.0	5.2	0.256	126.5	5.2	0.0	5.2
0.205	119.0	5.1	0.0	5.1	0.188	112.0	5.1	0.0	5.1
0.139	107.5	5.1	0.0	5.1	0.124	104.7	5.1	0.0	5.1
0.077	107.9	5.0	0.0	5.0	0.061	104.3	5.0	0.0	5.0
0.016	99.4	5.1	0.0	5.1	0.002	99.8	5.1	0.0	5.1
−0.042	101.8	5.0	0.0	5.0	−0.056	96.0	5.1	0.0	5.1
−0.098	84.5	5.0	0.0	5.0	−0.112	92.7	5.0	0.0	5.0
−0.153	97.8	5.1	0.0	5.1	−0.166	89.5	5.1	0.0	5.1
−0.206	96.1	5.1	0.0	5.1	−0.219	96.8	5.1	0.0	5.1
−0.258	84.3	5.2	0.0	5.2	−0.270	89.0	5.1	0.0	5.1
−0.308	83.2	5.2	0.0	5.2	−0.320	86.8	5.1	0.0	5.1
−0.357	93.5	5.2	0.0	5.2	−0.369	90.8	5.2	0.0	5.2
−0.405	84.1	5.2	0.0	5.2	−0.417	96.2	5.2	0.0	5.2
−0.452	92.2	5.4	0.0	5.4	−0.463	87.7	5.4	0.0	5.4
−0.498	91.9	5.6	0.0	5.6	−0.509	103.4	5.7	0.0	5.7
−0.543	105.7	5.9	0.0	5.9	−0.554	99.1	6.0	0.0	6.0
−0.587	117.4	6.2	0.0	6.2	−0.598	122.3	6.3	0.0	6.3
−0.630	126.6	6.6	0.0	6.6	−0.641	130.9	6.9	0.0	6.9
−0.673	139.1	7.3	0.0	7.3	−0.683	157.5	7.6	0.0	7.6
−0.714	178.6	7.8	0.0	7.8	−0.725	173.4	8.0	0.0	8.0
−0.755	182.5	8.7	0.0	8.7	−0.765	200.9	8.8	0.0	8.8
−0.796	233.2	9.3	0.0	9.3	−0.806	251.7	9.8	0.0	9.8
−0.835	280.8	10.0	0.0	10.0	−0.845	288.0	10.2	0.0	10.2
−0.874	289.2	11.0	3.5	11.6	−0.884	326.5	10.9	4.6	11.9
−0.913	350.5	11.7	9.0	14.8	−0.922	327.2	11.9	10.7	16.0
−0.951	377.0	12.3	17.0	21.0	−0.960	373.0	12.8	19.6	23.4
−0.988	439.5	13.2	28.6	31.5	−0.997	431.0	13.4	32.3	35.0

[a]) SD_{stat}, SD_{fit} and SD_{tot} are defined in subsect. 3.5. Both SD and $d\sigma/d\Omega$ are given in mb/sr.

In fig. 9, we present a sample of our data at 3.28 MeV which we compare with Alt's calculations [8]) at the same energy. In the same figure, "BNL trend" [ref. [1])] as well as Seagrave's data [13]) are plotted. One can conclude that Alt's calculations agree very well with the "BNL trend" at small angles but show more peaking at large angles where they are in good agreement with our data.

6. Conclusion

This work has produced many more cross section data than were available up

4

elastic cross section [a])

$\cos\theta_{c.m.}$	$d\sigma/d\Omega$	SD_{stat}	SD_{fit}	SD_{tot}	$\cos\theta_{c.m.}$	$d\sigma/d\Omega$	SD_{stat}	SD_{fit}	SD_{tot}
0.633	212.4	5.7	0.0	5.7	0.610	188.5	5.7	0.0	5.7
0.543	181.0	5.6	0.0	5.6	0.522	173.4	5.6	0.0	5.6
0.460	163.8	5.5	0.0	5.5	0.440	155.7	5.5	0.0	5.5
0.382	155.1	5.3	0.0	5.3	0.363	141.3	5.3	0.0	5.3
0.308	133.9	5.2	0.0	5.2	0.291	119.8	5.2	0.0	5.2
0.239	110.8	5.2	0.0	5.2	0.222	122.1	5.1	0.0	5.1
0.172	111.1	5.1	0.0	5.1	0.156	106.3	5.0	0.0	5.0
0.108	113.2	5.0	0.0	5.0	0.092	107.5	5.1	0.0	5.1
0.046	96.6	5.1	0.0	5.1	0.031	105.1	5.0	0.0	5.0
−0.013	101.2	5.1	0.0	5.1	−0.027	98.5	5.0	0.0	5.0
−0.070	91.2	5.1	0.0	5.1	−0.084	92.4	5.1	0.0	5.1
−0.126	96.8	5.1	0.0	5.1	−0.139	96.8	5.1	0.0	5.1
−0.180	92.4	5.0	0.0	5.0	−0.193	86.1	5.1	0.0	5.1
−0.232	98.4	5.1	0.0	5.1	−0.245	90.9	5.1	0.0	5.1
−0.283	89.5	5.0	0.0	5.0	−0.296	91.0	5.1	0.0	5.1
−0.333	86.3	5.1	0.0	5.1	−0.345	81.5	5.2	0.0	5.2
−0.381	89.2	5.2	0.0	5.2	−0.393	83.5	5.2	0.0	5.2
−0.429	93.9	5.4	0.0	5.4	−0.440	87.1	5.4	0.0	5.4
−0.475	89.7	5.5	0.0	5.5	−0.486	87.5	5.5	0.0	5.5
−0.520	99.0	5.7	0.0	5.7	−0.532	96.0	5.7	0.0	5.7
−0.565	105.8	6.0	0.0	6.0	−0.576	113.9	6.1	0.0	6.1
−0.609	122.4	6.6	0.0	6.6	−0.619	123.7	6.7	0.0	6.7
−0.651	136.8	7.0	0.0	7.0	−0.662	137.3	7.0	0.0	7.0
−0.693	155.2	7.5	0.0	7.5	−0.704	162.1	7.7	0.0	7.7
−0.735	185.8	8.3	0.0	8.3	−0.745	200.4	8.5	0.0	8.5
−0.775	221.5	8.8	0.0	8.8	−0.786	208.5	8.9	0.0	8.9
−0.815	252.8	9.9	0.0	9.9	−0.825	265.6	9.9	0.0	9.9
−0.855	297.3	10.4	1.7	10.5	−0.865	298.0	10.9	2.6	11.2
−0.894	332.7	11.4	5.8	12.8	−0.903	352.1	11.5	7.2	13.6
−0.932	365.4	12.0	12.4	17.3	−0.941	382.3	12.2	14.7	19.1
−0.969	409.8	12.6	22.5	25.8	−0.979	410.6	12.7	25.1	28.2

to now and has shown that, statistically speaking, partial waves as high as $l = 3$ and $l = 5$ were indeed necessary in the parametrization of the scattering amplitudes at 2.48 and 3.28 MeV, respectively. Moreover it has shown that the (n, d) cross section, in this energy range, is more peaked at large angles than suggested by earlier data. This is in agreement with three body calculations. These data should help in getting more reliable phase shifts for the n-d elastic scattering at low energy.

We would like to express our appreciation to the computer center of the EPF-Lausanne for providing many hours of computer time. We would also like to thank

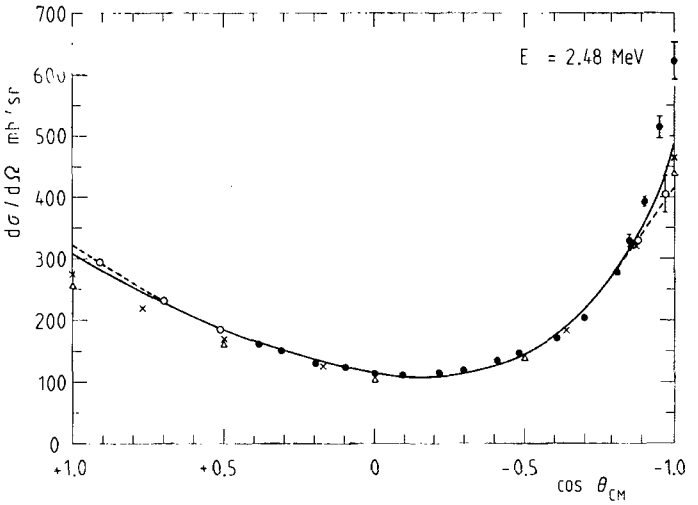

Fig. 8. Comparison between experiment and theory. The solid line is from fig. 7 of ref. [8]), $E = 2.45$ MeV; the dashed line the "BNL trend" of ref. [1]), $E = 2.45$ MeV; crosses from Fayard [20]), $E = 2.6$ MeV; triangles from Fuda and collaborators [18, 19]), $E = 2.45$ MeV; open circles, some of Seagrave's data [13]), $E = 2.45$ MeV; and solid circles the present experiment, $E = 2.48$ MeV. The error bars are equal to SD_{tot} (subsect. 3.5).

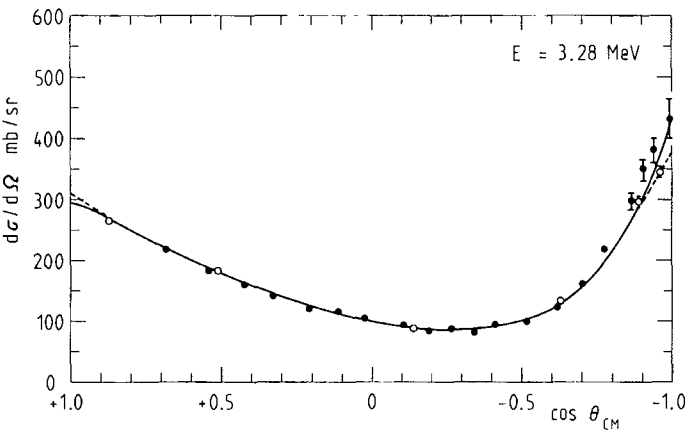

Fig. 9. Comparison between experiment and theory. The solid line is from fig. 8 of ref. [8]), $E = 3.27$ MeV; the dashed line the "BNL trend" of ref. [1]); open circles, some of Seagrave's data [13]), $E = 3.27$ MeV; and solid circles the present experiment, $E = 3.28$ MeV. The error bars are equal to SD_{tot} (subsect. 3.5).

Mrs. J. Moret of the Neuchâtel University computer center, for her help in running the SPSS code. Discussions with Dr. E. Schwarz have been of valuable help.

Appendix

When one fits the polynomial

$$Y = \sum_{j=0}^{n} a_j X_j(x)$$

to a set of data $y_1 \ldots y_N$ one knows that the following matrix equation holds [14]):

$$(a) = (\varepsilon)\left[(X)\left(\frac{1}{\sigma^2}\right)(y)\right],$$

where (a) is the column matrix of the coefficients a_j, $(\varepsilon) = [(X)(1/\sigma^2)(\tilde{X})]^{-1}$ is the "error matrix" that is the variance-covariance matrix of the coefficients a_j, (X) is the matrix built with the $(n+1) \times N$ values of $X_j(x_i)$, $j = 0, \ldots, n$; $i = 1 \ldots N$, $(1/\sigma^2)$ is the diagonal matrix of order $N \times N$ built with the N values of the variance of the data Y_i, and (Y) is the column matrix made out of the N experimental data Y_i.

Condition (c) of subsect. 3.6 is fulfilled by our procedure since ε depends only on (X) and $(1/\sigma^2)$, since we have extracted the new data at the same points where the original data were found, and since their variances σ_i^2 have been computed in a way so as to be coherent with the variances of the original data.

The fact that the equation for (a) results from a least square formalism and the fact that we produced the new set of data through sampling Gaussian distributions, can justify that condition (b) of the same subsection is also fulfilled. A few tests showed us that it was indeed the case. The same argument holds to justify condition (a) of that subsection.

References

1) M. D. Goldberg, V. M. May and J. R. Stehn, Brookhaven National Laboratory report BNL-400, vol. I (1962)
2) R. S. Christian and J. L. Gammel, Phys. Rev. **91** (1953) 100
3) W. T. H. Van Oers and R. W. Brockman, Nucl. Phys. **A92** (1967) 561
4) J. Arvieux, Nucl. Phys. **A221** (1974) 253
5) S. Jaccard, J. Piffaretti, R. Viennet and J. Weber, Proc. Third Int. Symp. on polarization in nuclear reactions, Madison, 1970, ed. H. H. Barshall and W. Haeberli (The University of Madison Press, Madison, 1971) p. 448
6) D. Bovet, P. Chatelain, S. Jaccard, Y. Onel, J. Piffaretti, R. Viennet and J. Weber, Proc. Int. Conf. on the interaction of neutron with nuclei, Lowell, 1976, ed. E. Sheldon (Techn. Inf. Center, ERDA, CONF-760715-P2) part 2, p. 1357
7) D. Bovet, P. Chatelain, R. Viennet and J. Weber, J. of Phys. **G4** (1978) 1313
8) E. O. Alt and B. L. G. Bakker, Z. Phys. **A273** (1975) 37

9) V. Morgan and R. L. Walter, Phys. Rev. **168** (1968) 1114
10) P. Chatelain, Y. Onel and J. Weber, Nucl. Instr. **151** (1978) 519
11) G. Pisent, Helv. Phys. Acta **36** (1963) 248
12) S. Jaccard, Thesis, Université de Neuchâtel (1973)
13) J. D. Seagrave and L. Cranberg, Phys. Rev. **105** (1957) 1816
14) D. J. Hudson, Statistics lectures II, CERN report, CERN-64-18 (1964);
P. R. Bevington, in Data reduction and error analysis for the physical sciences (McGraw-Hill, New-York, 1969)
15) Statistical package for the social sciences, 2nd ed. (McGraw-Hill, New-York, 1975)
16) J. D. Seagrave and R. L. Henkel, Phys. Rev. **98** (1955) 666
17) B. Sundqvist, Proc. Int. Conf. on few body systems and nuclear forces, vol. 2, Graz 1978, ed. H. Zingl, M. Haftel and H. Zankel (Springer-Verlag, Berlin, Heidelberg, 1978)
18) M. G. Fuda and B. A. Girard, Phys. Rev. **C17** (1978) 1
19) J. S. Whiting and M. G. Fuda, Phys. Rev. **C14** (1976) 18
20) C. Fayard, private communication (1976)
21) B. L. G. Bakker, Z. Phys. **A272** (1975) 335
22) E. O. Alt, W. Sandhas, H. Zankel and H. Ziegelmann, Phys. Rev. Lett. **37** (1976) 1537